Hindawi Publishing Corporation
Journal of Nanomaterials
Volume 2011, Article ID 837123, 5 pages
doi:10.1155/2011/837123

Research Article

Core-Shell Nanostructure of α-Fe_2O_3/Fe_3O_4: Synthesis and Photocatalysis for Methyl Orange

Yang Tian,[1] Di Wu,[1] Xiao Jia,[2] Binbin Yu,[1] and Sihui Zhan[3]

[1] *Department of Chemistry, Capital Normal University, Beijing 100048, China*
[2] *Institute of Functional Materials, College of Chemistry and Chemical Engineering, Fuzhou University, Fujian 350002, China*
[3] *College of Environmental Science and Engineering, Nankai University, Tianjin 300071, China*

Correspondence should be addressed to Yang Tian, tianyang@mail.sdu.edu.cn

Received 9 April 2010; Accepted 1 June 2010

Academic Editor: William W. Yu

Fe_3O_4 nanoparticle was synthesized in the solution involving water and ethanol. Then, α-Fe_2O_3 shell was produced in situ on the surface of the Fe_3O_4 nanoparticle by surface oxidation in molten salts, forming α-Fe_2O_3/Fe_3O_4 core-shell nanostructure. It was showed that the magnetic properties transformed from ferromagnetism to superparamagnetism after the primary Fe_3O_4 nanoparticles were oxidized. Furthermore, the obtained α-Fe_2O_3/Fe_3O_4 core-shell nanoparticles were used to photocatalyse solution of methyl orange, and the results revealed that α-Fe_2O_3/Fe_3O_4 nanoparticles were more efficient than the self-prepared α-Fe_2O_3 nanoparticles. At the same time, the photocatalyzer was recyclable by applying an appropriate magnetic field.

1. Introduction

Owing to their tunable properties and large surface-to-volume ratios, nanocrystals (NCs) are being considered for a wide range of applications including photovoltaics, biomedicalimaging, photocatalysts, and optoelectronics [1–4]. Nanocrystal heterostructures (NCHs) are an emerging subclass of NCs where two or more chemically distinct components are brought together epitaxially [5]. The best known example is the core/shell structure where the outer shell enhances the properties of the core (e.g., increasing photoluminescence quantum yields of CdSe NCs with ZnS or CdS shell [6, 7]. These core-shell nanostructures expand single-component nanoparticles to hybrid nanostructures with discrete domains of different materials arranged in a controlled fashion. Thus, different functionalities can be integrated, with the dimension and material parameters of the individual components optimized independently even providing entirely novel properties via the coupling between different components. In view of the scientific importance of these materials, it is not surprising that a wide variety of approaches for their synthesis have been reported [8–13]. Specifically, the surface oxidation method has attracted much attention because it could be utilized as a simplistic route to obtain core/shell nanostructures [11, 12].

Magnetic separation provides a convenient method for removing and recycling magnetized species by applying an appropriate magnetic field. So, magnetic nanoparticles combining with catalysts could not only increase the durability of the catalysts but also help to separate and recycle the catalyst particles. For example, magnetic nanoparticles have been immobilized in a mesoporous silica shell with molybdenum oxide forming a magnetically recyclable epoxidation catalyst [14]. A core-shell structure of TiO_2/$BaFe_{12}O_{19}$ composite nanoparticle that can photodegrade organic pollutants in the dispersion system effectively and can be recycled easily by a magnetic field was also reported [15]. Another magnetically separable photocatalyst TiO_2/SiO_2/$NiFe_2O_4$ (TSN) nanosphere with egg-like structure was prepared by Xu et al. [16]. However, there are few reports on the magnetic nanoparticles integrating with lower cost photocatalysis, α-Fe_2O_3 for the photodegradation [17–19]. Here, we fabricated α-Fe_2O_3/Fe_3O_4 core-shell nanostructures by a surface oxidation method on the surface of primary Fe_3O_4 nanoparticles in molten salts, which showed high efficiency and good recycling for photocatalysis of methyl orange (MO).

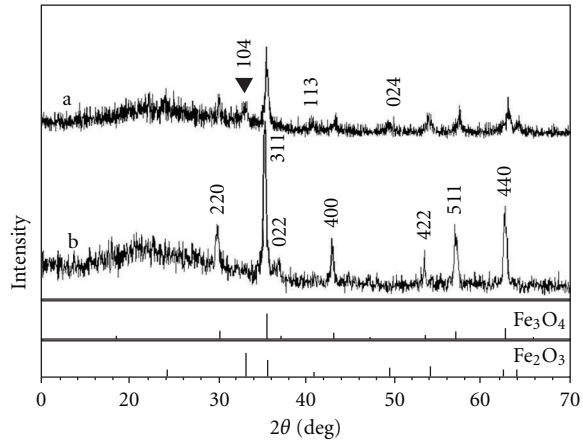

Figure 1: XRD patterns of the obtained α-Fe_2O_3/Fe_3O_4 (a) and Fe_3O_4 (b).

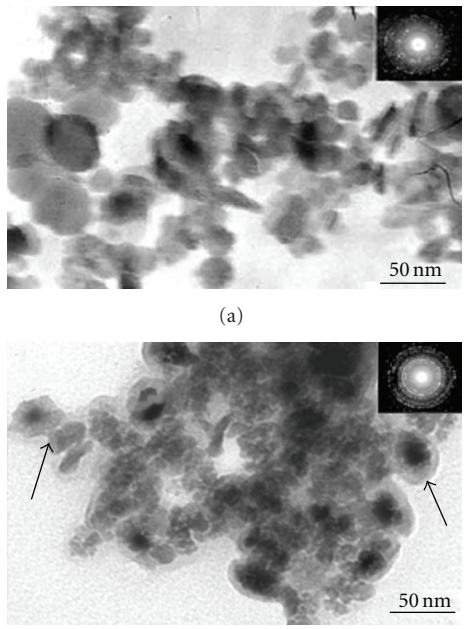

Figure 2: TEM image of the obtained primary Fe_3O_4 nanoparticles (a) and α-Fe_2O_3/Fe_3O_4 nanoparticles (b), the insets are SAED patterns of them, respectively.

2. Experiments

2.1. Synthesize of Primary Fe_3O_4 Nanoparticles. All the chemicals were analytically pure and used without purifying further. In a 250 mL three-neck flask, sodium nitrate (0.5 g, Shanghai Chemical Reagent) and ferrous (II) sulfate (1.6 g, Shanghai Chemical Reagent) were dissolved in a mixture solution of distilled water (30 mL) and absolute ethanol (30 mL, Shanghai Chemical Reagent) under a vacuum surround. On the other hand, sodium hydroxide (1 g, Tianjin Chemical Reagent) was dissolved in 10 mL distilled water and then was injected into the three-neck flask by an injector under magnetic stirring. The reaction lasted for about 10

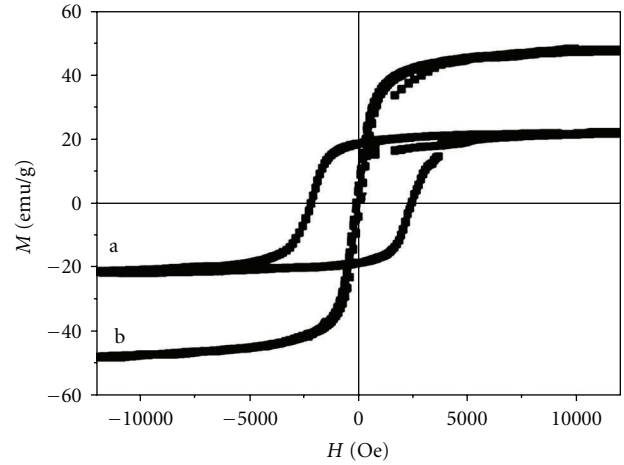

Figure 3: Magnetic hysteresis loops for the Fe_3O_4 nanoparticles (a) and α-Fe_2O_3/Fe_3O_4 (b)

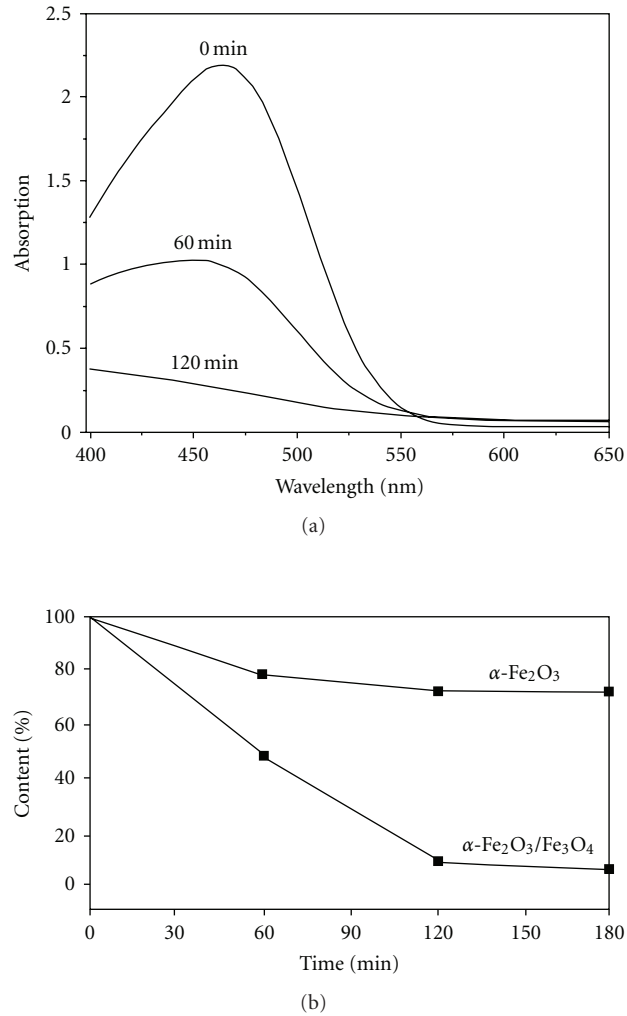

Figure 4: Absorption spectra (a) of the MO solution for 0 min, 60 min and 120 min, and photocatalysis performance (b) of the core-shell sample and α-Fe_2O_3 sample.

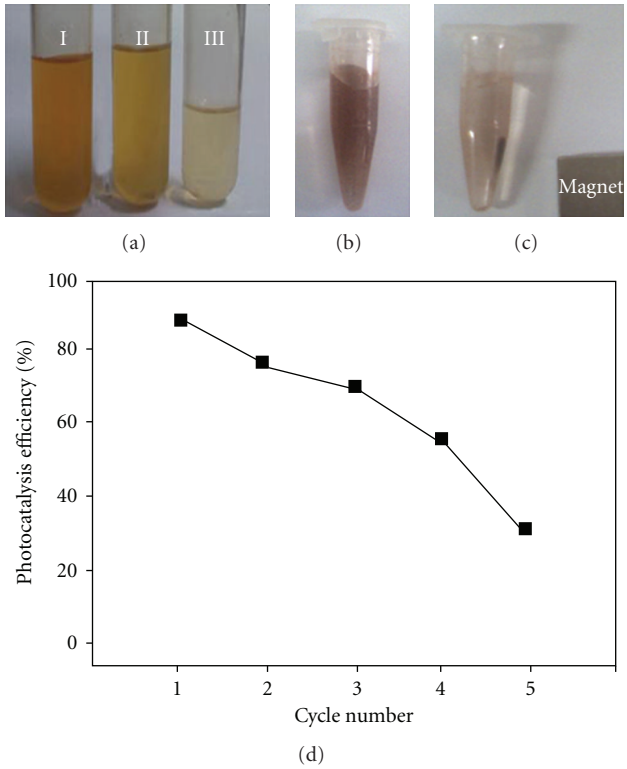

Figure 5: Optical image (a) of the MO solution after photocatalysis lasted 0 min, 60 min, and 120 min (b) and (c) are the optical images of the catalyst being separated by a magnet; (d) is efficiency curve for multiple cycles of photocatalysis.

minutes in a vacuum surround under strong stirring until the white precipitate became black. The obtained black precipitate was collected by centrifugation separating and then was washed with distilled water for 4 times. Finally the precipitate was dried at 80°C for 12 hours to obtain the Fe_3O_4 nanoparticles.

2.2. Synthesis of α-Fe_2O_3/Fe_3O_4. Sodium nitrate (4.2 g) and potassium nitrate (2.5 g) were mixed in a crucible (30 mL) and heated up to 310°C to melt. The obtained Fe_3O_4 nanoparticles were put into the crucible to react for 30 minutes, and then the molten salt was cooled to room temperature. The product was obtained by washing the fusion with deionized water to remove the nitrates and filtration for three times. Finally, the precipitate was dried at 80°C for 12 hours to obtain the α-Fe_2O_3/Fe_3O_4 nanoparticles.

2.3. Measurement of Photocatalytic Activity. The evaluation of photocatalytic activity for the prepared samples decolorizing MO aqueous solution was performed at ambient temperature. The obtained α-Fe_2O_3/Fe_3O_4 core-shell catalyst (0.02 g) was placed into a tubular quartz reactor of 100 mL 20 mg/L MO aqueous solution. The reactor was surrounded with a UV lamp (125 W) with stirring. After the reaction began, the mixture was sampled at different times and separated by a magnet to discard any sediment. Then, absorption spectra were obtained through a wavelength scan on a UV-Vis spectrophotometer.

2.4. Characterization. The X-ray diffraction (XRD) patterns of the samples were collected using a diffractometer (Rigaku D/Max 2200PC) with CuKα radiation (λ = 1.5418 Å) and graphite monochromator from 10 to 80° at a scanning rate 5.0°/min. Unit cell dimensions were determined in the JADE 5 program for X-ray diffraction pattern processing, identification, and quantification. The size and morphology of the products were characterized by transmission electron microscopy (TEM, JEM100-CXII) with the potential of performing selected-area electron diffraction (SAED). Magnetometry measurements were taken with a Quantum Design PPMS SQUID magnetometer. The absorption spectra of MO solution were obtained by a UV-vis spectrophotometer (Shimadzu UV-vis 2550).

3. Results and Discussion

To form α-Fe_2O_3/Fe_3O_4 core-shell nanostructure, the appropriate reaction conditions were explored in our work as shown in Table 1. It reveals that when the primary Fe_3O_4 nanoparticles were obtained in water without ethanol, they were difficultly oxidized into α-Fe_2O_3 even in molten salts of 380°C for 30 min; however, when the primary Fe_3O_4 nanoparticles were obtained in 20 mL H_2O and 40 mL ethanol (the content of ethanol was 2/3), they were oxidized into α-Fe_2O_3 completely without Fe_3O_4 leaving even in 310°C for only 10 min (Figure S1(a) in Supplementary Material available online at doi: 10.1155/2011/837123). When the primary Fe_3O_4 nanoparticles were obtained in 30 mL H_2O and 30 mL ethanol (the content of ethanol was 1/2), they could be oxidized partially forming α-Fe_2O_3/Fe_3O_4 core-shell nanostructure in 310°C for 30 min (Figure 1(a)) but oxidized completely in 380°C for only 10 min (Figure S1(b) in Supplementary Material available online at doi: 10.1155/2011/837123). So, increasing the content of ethanol in the solution for preparing Fe_3O_4 nanoparticles is beneficial to subsequent oxidation reaction of Fe_3O_4 to form α-Fe_2O_3/Fe_3O_4 core-shell nanostructure. However, excess ethanol over 1/2 content would result in complete and rapid oxidization of Fe_3O_4 nanoparticles in our molten salts, which went against forming core-shell structure. This phenomenon could be explained from XRD patterns of the prepared Fe_3O_4 (Figure S2 and Figure 1(b)) which show that the crystallization grew lower as the content of ethanol was enhanced. It is obvious that the crystallized Fe_3O_4 well is more stable and difficult to oxidize into α-Fe_2O_3.

To characterize phase and crystallization of the products, powder X-ray diffraction (XRD) was performed from the obtained α-Fe_2O_3/Fe_3O_4 and Fe_3O_4 samples. The XRD pattern for Fe_3O_4 nanoparticles (Figure 1(b)) shows that all the peaks are in good agreement with the cubic structure [space group: *Fd-3m*] known from Fe_3O_4 crystal (JCPDS Card 65-3107), meaning its high crystallization and few impurities. The crystal cell dimension of the sample is calculated to be a = 0.8396 nm by Jade 5, which is accorded with the

Table 1: Different samples obtained from adjusting reaction conditions: different molar ratios of H_2O and EtOH, oxidation temperature, and oxidation time.

Sample	H_2O/mL	EtOH/mL	Primary product	Oxidation Temp./°C	Oxidation Time/min	Oxidation product
S1	60	0	Fe_3O_4	380	30	Fe_3O_4
S2	30	30	Fe_3O_4	380	10	α-Fe_2O_3
S3	30	30	Fe_3O_4	310	30	α-Fe_2O_3/Fe_3O_4
S4	20	40	Fe_3O_4	310	10	α-Fe_2O_3

value given in the JCPDS Card 65-3107 file for Fe_3O_4 (a = 0.8391 nm). Furthermore, according to the full width at half maximum (FWHM) of (121) reflections, the average size of the crystalline particles for the primary Fe_3O_4 is calculated to be 30.7 nm based on the Debye-Scherrer formula. Figure 1(a) is the XRD pattern for the α-Fe_2O_3/Fe_3O_4 obtained from surface oxidation of Fe_3O_4 in molten salt. It reveals that these nanoparticles were composed of cubic-structured Fe_3O_4 and α-Fe_2O_3 (JCPDS No. 04-0784).

Figure 2(a) shows the representative TEM image of the obtained Fe_3O_4 nanoparticles. It shows that the sizes of nanocrystals are about 20–50 nm but not uniform, which is roughly closed to the average size resulted from the Debye-Scherrer formula. The inset of Figure 2(a) is corresponding SAED pattern, exhibiting the high crystalline nature of cubic-phase Fe_3O_4. Figure 2(b) is TEM image of the α-Fe_2O_3/Fe_3O_4, which shows clear core-shell nanostructure for the sample. Furthermore, it shows the size of Fe_3O_4 core decrease to be about 15–30 nm.

The magnetic properties of the as-prepared α-Fe_2O_3/Fe_3O_4 and Fe_3O_4 nanoparticles were investigated with a Quantum magnetometer at room temperature. The magnetic hysteresis loop (curve a in Figure 3) for the Fe_3O_4 nanoparticles indicates their ferromagnetism at room temperature. The coercivity (Hc) is shown to be about 2330 Oe, the saturation magnetization (Ms) is 22.6 emu/g, and the remnant magnetization (Mr) is 18.9 emu/g. However, the hysteresis loop of the obtained α-Fe_2O_3/Fe_3O_4 nanostructure shows near superparamagnetism at room temperature, which is different from the primary Fe_3O_4 nanoparticles distinctly. It is well known that the surface spin disorder enhancing caused by the decreasing of particles size [20] and the coercivity would approach zero under a short thermal fluctuation (so-called super paramagnetism) if the crystal size is small enough. Thus, the transformation from ferromagnetism to superparamagnetism indicates the average size decrease when the primary Fe_3O_4 nanoparticles became into the Fe_3O_4 cores of α-Fe_2O_3/Fe_3O_4, which is accorded with the result of TEM. At the same time, it reveals that the saturation magnetization (Ms) for Fe_3O_4 cores of α-Fe_2O_3/Fe_3O_4 nanoparticles is about 48.7 emu/g, and the remnant magnetization (Mr) is about 8.6 emu/g.

To evaluate the potential application in water treatment of the obtained α-Fe_2O_3/Fe_3O_4 complex nanostructure, the photocatalysis capacities for the organic pollutant were investigated. Here, MO was chosen as the model organic pollutant. The initial concentration of the MO solution was set to be 20 mg/L. Figure 4(a) shows the visible absorption spectra of for MO solution by the degradation of complex nanostructured α-Fe_2O_3/Fe_3O_4 with different time. The spectra show that the concentration of MO decreased to 54.4% after reacted for 60 min comparing the original concentration, and the maximum removal capacity of the photocatalysis reached about 90.1% in a time period of 120 min. At the same time, additional experiments were made to compare the photocatalysis performance between the core-shell sample (S3 of Table 1) and α-Fe_2O_3 sample (S2 of Table 1) at the entirely same photocatalysis conditions. As shown in Figure 4(b), the α-Fe_2O_3/Fe_3O_4 core-shell nanostructure behaved higher photocatalysis efficiency for MO. The rapid removal of MO may be associated with the electrostatic attraction between the α-Fe_2O_3 shell and Fe_3O_4 core of the complex nanostructure. Under the ultraviolet radiation, electrons in the valence band (CB) of α-Fe_2O_3 were excited to its conduction band (CB), with same amount of holes left in VB. Driven by the decreased potential energy band gap of α-Fe_2O_3 is ~2.20 eV and band gap of Fe_3O_4 is ~0.10 eV), the photogenerated electrons in CB of α-Fe_2O_3 tended to transfer to that of Fe_3O_4. So, the photogenerated electrons and holes were separated at the α-Fe_2O_3/Fe_3O_4 interfaces, which reduced their recombination probability, and enhanced the efficiency of generating hydroxyl radicals.

Figure 5(a) is the optical image for the MO solution with different photocatalysis time, which shows the solution became clear gradually from I to III by photocatalysis. Furthermore, the used catalyst of α-Fe_2O_3/Fe_3O_4 nanostructure could be recycled by a magnet. Figure 5(b) and 5(c) shows the optical image of the catalyst being separated by a magnet. So, the photocatalyst could be recycled by a magnetic field, which would be assistance to the recycle of the photocatalyst. Furthermore, to study the recyclability of the photocatalyzer, experiments in multiple cycles of photocatalysis plus magnetic separation were performed, and it revealed that the photocatalyzer owned good recyclability as shown in Figure 5(d).

4. Conclusion

In summary, we fabricated Fe_3O_4 nanoparticles in a mixture solution of water and ethanol, and then α-Fe_2O_3 shell was produced in situ on the surface of the Fe_3O_4 nanoparticle by surface oxidation to form α-Fe_2O_3/Fe_3O_4 core-shell nanostructure in molten salts. To remove MO in the water by our α-Fe_2O_3/Fe_3O_4 core-shell nanostructure showed better photocatalysis property. At the same time, the photocatalyst could be recycled by the magnetic field, which would be

assistance to the recycle of the photocatalyst. These studies not only enrich the contents of core-shell nanostructure chemistry but also are beneficial to investigate their potential application in photocatalysis.

Acknowledgments

This work is supported by the Beijing Natural Science Foundation (Grant no. 2103048), Natural Science Foundation of China (Grant no. 20907022), and Funding Project for Academic human Resources Development in Institutions of Higher Learning Under the Jurisdiction of Beijing Municipality (PHR20100718).

References

[1] P. V. Kamat, "Meeting the clean energy demand: nanostructure architectures for solar energy conversion," *Journal of Physical Chemistry C*, vol. 111, no. 7, pp. 2834–2860, 2007.

[2] X. Michalet, F. F. Pinaud, L. A. Bentolila et al., "Quantum dots for live cells, in vivo imaging, and diagnostics," *Science*, vol. 307, no. 5709, pp. 538–544, 2005.

[3] X. Chen and S. S. Mao, "Titanium dioxide nanomaterials: synthesis, properties, modifications and applications," *Chemical Reviews*, vol. 107, no. 7, pp. 2891–2959, 2007.

[4] J. Zhao, J. A. Bardecker, A. M. Munro et al., "Efficient CdSe/CdS quantum dot light-emitting diodes using a thermally polymerized hole transport layer," *Nano Letters*, vol. 6, no. 3, pp. 463–467, 2006.

[5] P. D. Cozzoli, T. Pellegrino, and L. Manna, "Synthesis, properties and perspectives of hybrid nanocrystal structures," *Chemical Society Reviews*, vol. 35, no. 11, pp. 1195–1208, 2006.

[6] B. O. Dabbousi, J. Rodriguez-Viejo, F. V. Mikulec et al., "(CdSe)ZnS core-shell quantum dots: synthesis and characterization of a size series of highly luminescent nanocrystallites," *Journal of Physical Chemistry B*, vol. 101, no. 46, pp. 9463–9475, 1997.

[7] X. Peng, M. C. Schlamp, A. V. Kadavanich, and A. P. Alivisatos, "Epitaxial growth of highly luminescent CdSe/CdS core/shell nanocrystals with photostability and electronic accessibility," *Journal of the American Chemical Society*, vol. 119, no. 30, pp. 7019–7029, 1997.

[8] L. Wang, H.-Y. Park, S. I.-I. Lim et al., "Core@shell nanomaterials: gold-coated magnetic oxide nanoparticles," *Journal of Materials Chemistry*, vol. 18, no. 23, pp. 2629–2635, 2008.

[9] Z. Sun, Z. Yang, J. Zhou et al., "A general approach to the synthesis of gold-metal sulfide core-shell and heterostructures," *Angewandte Chemie*, vol. 48, no. 16, pp. 2881–2885, 2009.

[10] T. Zhou, M. Lu, Z. Zhang, H. Gong, W. S. Chin, and B. Liu, "Synthesis and characterization of multifunctional FePt/ZnO core/shell nanoparticles," *Advanced Materials*, vol. 21, no. 3, pp. 403–406, 2009.

[11] A. C. Johnston-Peck, J. Wang, and J. B. Tracy, "Synthesis and structural and magnetic characterization of Ni(Core)/NiO(Shell) nanoparticles," *ACS Nano*, vol. 3, no. 5, pp. 1077–1084, 2009.

[12] C. Wang, D. R. Baer, J. E. Amonette, M. H. Engelhard, J. Antony, and Y. Qiang, "Morphology and electronic structure of the oxide shell on the surface of iron nanoparticles," *Journal of the American Chemical Society*, vol. 131, no. 25, pp. 8824–8832, 2009.

[13] S. Sacanna and A. P. Philipse, "A generic single-step synthesis of monodisperse core/shell colloids based on spontaneous pickering emulsification," *Advanced Materials*, vol. 19, no. 22, pp. 3824–3826, 2007.

[14] M. Shokouhimehr, Y. Piao, J. Kim, Y. Jang, and T. Hyeon, "A magnetically recyclable nanocomposite catalyst for olefin epoxidation," *Angewandte Chemie*, vol. 46, no. 37, pp. 7039–7043, 2007.

[15] W. Fu, H. Yang, M. Li et al., "Preparation and photocatalytic characteristics of core-shell structure $TiO_2/BaFe_{12}O_{19}$ nanoparticles," *Materials Letters*, vol. 60, no. 21-22, pp. 2723–2727, 2006.

[16] S. Xu, W. Shangguan, J. Yuan, M. Chen, J. Shi, and Z. Jiang, "Synthesis and performance of novel magnetically separable nanospheres of titanium dioxide photocatalyst with egg-like structure," *Nanotechnology*, vol. 19, no. 9, Article ID 095606, 2008.

[17] S.-W. Cao and Y.-J. Zhu, "Hierarchically nanostructured α-Fe_2O_3 hollow spheres: preparation, growth mechanism, photocatalytic property, and application in water treatment," *Journal of Physical Chemistry C*, vol. 112, no. 16, pp. 6253–6257, 2008.

[18] X.-L. Fang, C. Chen, M.-S. Jin et al., "Single-crystal-like hematite colloidal nanocrystal clusters: synthesis and applications in gas sensors, photocatalysis and water treatment," *Journal of Materials Chemistry*, vol. 19, no. 34, pp. 6154–6160, 2009.

[19] E. Montiel-Palacios, A. K. Medina-Mendoza, A. Sampieri, C. Angeles-Chávez, I. Hernández-Pérez, and R. Suarez-Parra, "Photo-catalysis of phenol derivatives with Fe_2O_3 nanoparticles dispersed on SBA-15," *Journal of Ceramic Processing Research*, vol. 10, no. 4, pp. 548–552, 2009.

[20] Y. Tian, D. Chen, and X. Jiao, "$La_{1-x}Sr_xMnO_3$ (x = 0, 0.3, 0.5, 0.7) nanoparticles nearly freestanding in water: preparation and magnetic properties," *Chemistry of Materials*, vol. 18, no. 26, pp. 6088–6090, 2006.